

ESTIMATING THE MAGNITUDE AND PHASE RESPONSE OF A 50 GHz SAMPLING OSCILLOSCOPE USING THE “NOSE-TO-NOSE” METHOD^a

Paul D. Hale, Tracy S. Clement, Kevin J. Coakley^b, C. M. Wang^b, Donald C. DeGroot^c, and Angelo P. Verdoni

National Institute of Standards and Technology
Optoelectronics Division
325 Broadway, Boulder, Colorado 80303
e-mail: hale@boulder.nist.gov
(303) 497-5367

Abstract

We describe estimation of the magnitude and phase response of a sampling oscilloscope with 50 GHz bandwidth using the nose-to-nose method. The measurements are corrected for the non-ideal properties of the oscilloscope and calibration apparatus, including mismatch and time-base distortion, drift, and jitter. The mean and standard deviation of repeated measurements of an ensemble of three oscilloscope samplers are reported, along with attempts to verify the magnitude calibration using a swept sine-wave method.

Introduction

The frequency-dependent phase and magnitude response of a linear device uniquely determine its time-domain response and are used in optoelectronic device metrology, nonlinear device metrology, and high-speed digital circuit design. Frequency-domain network analyzers measure device magnitude and phase responses relative to a reference tone, but cannot measure the total phase relationship of the frequency components in a broadband waveform. Here time-domain methods are required. We are investigating the use of a high-speed sampling oscilloscope, which has been calibrated using the nose-to-nose (n2n) method^{1,2}, to measure the phase response of fast optical detectors and electrical comb generators. In this paper we describe efforts to calibrate the magnitude and phase response of an oscilloscope using n2n, and to verify this calibration method. We also describe various corrections for non-ideal adapters and time-base and the integration of these corrections into the calibration procedure.

The idea behind n2n is described by Rush and Verspecht^{1,2}. A

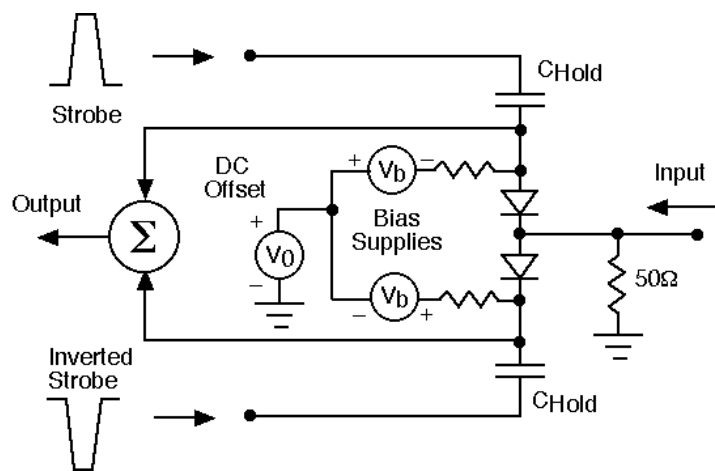


Fig. 1. Simplified schematic diagram of the two-diode sampler circuit³. V_b is the diode reverse bias voltage. Kick out pulses are generated at the input port when the DC offset voltage V_0 is nonzero.

^a Publication of the U. S. Government, not subject to U. S. copyright.

^b Statistical Engineering Division

^c Radio-Frequency Technology Division

simplified schematic of the sampler circuit geometry is shown in Fig. 1. The sampler also includes a transmission line and 2.4 mm (male) coaxial connector on the input port. The sampler diodes are normally reverse biased and the offset voltage $V_0 = 0$. The strobe pulse forces the sampling diodes into conduction. Short current pulses conducted through the sampling diodes collide at the sampling node and cancel because of the symmetry of the system. When an offset $V_0 \neq 0$ is added to the diode bias voltage, the currents no longer cancel and a short pulse leaks out of the input port. According to the n2n theory, the pulse that leaks out, called the “kick-out” pulse, is proportional to the “impulse response” (defined in ref. [3]) of the sampler that generated it. If the kick-out generator is connected to a similar sampler, called the receiver, the measured waveform is the convolution of the kick-out pulse with the impulse response of the second sampler. If combinations of three samplers are measured, the impulse response of any one sampler can be estimated by solving a set of three equations in three unknowns. Preliminary simulations³ at NIST indicate that the kick-out pulse is

a reasonably accurate estimate of the sampler impulse response for certain circuit parameters. Investigation of the parameter space for which the n2n assumptions hold is an area of continuing research⁴. Actual measurements providing the estimate of the impulse response of a sampling oscilloscope are affected by various non-ideal properties of the hardware. Calibration of an oscilloscope's frequency response requires estimation and correction of these effects, which include distortion, drift, and jitter components in the time-base, and electrical mismatch. A basic flow chart for the calibration procedure is shown in Fig. 2. Time-base distortion (TBD) is a deterministic error in the delay generator that triggers a sample. Drift and jitter are random variations in the sample time which occur on a long and short time scale relative to one complete sweep of the display. Many waveforms must be averaged to achieve a low noise level.

Nose-to-nose measurements and time-base drift correction

We next describe the experimental setup for measuring the n2n signal. The samplers of the two oscilloscopes are positioned “nose-to-nose” and connected via a single 2.4 mm female-female adapter. Combinations of three samplers are measured to estimate the impulse response of each sampler.

Synchronization and timing of the generator and receiver are critical. The pair must be configured so that the receiver is sampling only when a kick-out pulse is present. A synthesized signal generator generates a TTL-compatible square-wave at 2.4 kHz and triggers a step-pulse generator. The resulting pulse has a fall time of about 15 ps. The step-pulse is attenuated and split to give a trigger signal for both oscilloscopes. We have found that increasing the fall time to greater than about 100 ps increases the observed jitter significantly. The time-base of the generator scope is set such that it produces a kick-out pulse about 56 ns after the trigger pulse, positioning the received pulse at about 63.4 ns in a 4 ns window that starts at 63 ns. The generator oscilloscope is set to take 16 samples per 0.4 ms sweep. Oscilloscope control and data

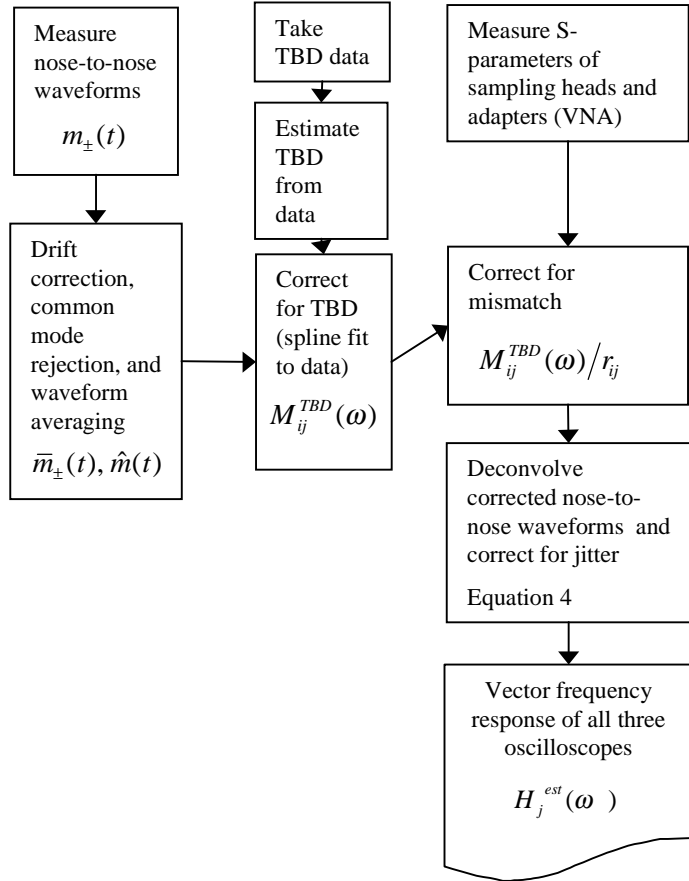


Fig. 2. Flow chart of nose-to-nose procedure.

acquisition are performed by a desktop computer. Each measured waveform is saved for post-processing. Acquisition of 1000 waveform pairs takes about 45 minutes. During the measurement process the time-base may drift about 1 to 2 ps, producing significant error at high frequencies. Consequently, we must carefully estimate and correct for drift.

The measured signal actually contains the kick-out pulse $k(t)$ and a strobe leakage signal $c(t)$ produced by sampler diode imbalance, sampler asymmetry, and capacitive coupling. By reversing the offset, the sign of the kick-out can be changed without changing the sign of the leakage. We alternately measure the signal for both positive and negative 100 mV offsets. This offset is chosen as a compromise between poor signal-to-noise ratio and sampler nonlinearity. In the ideal noise-free case, for positive offset we observe $m_+(t) = (k(t) + c(t)) * h(t)$. With negative offset, we observe $m_-(t) = (-k(t) + c(t)) * h(t)$. By differencing the two measurements, and dividing by 2, we estimate the signal of interest. In practice, we measure many noisy realizations of the “plus” and “minus” signals. Due to instrument drift, the “plus” signals are misaligned with respect to one another. Likewise, the noisy “minus” signals are misaligned with respect to each other. We estimate the relative shift of the n th “plus” signal with respect to the first “plus” signal by cross-correlation analysis of all pairs of signals. Similarly, we estimate the relative shift of the n th “minus” signal with respect to the first “minus” signal by all-pairs cross-correlation analysis. We then compute the averages of the aligned plus signals $\bar{m}_+(t)$ and the aligned minus signals $\bar{m}_-(t)$. Because the “plus” and “minus” signals are aligned independently, $\bar{m}_+(t)$ and $\bar{m}_-(t)$ may be misaligned. Our estimate of the relative shift of the two signal averages is the difference in the mean values of the “plus” signal relative shifts $\bar{\tau}_+$ and the mean values of the “minus” relative shifts $\bar{\tau}_-$. Finally, our estimate of the signal of interest is

$$\hat{m}(t) = \frac{1}{2} \{ \bar{m}_+(t - \bar{\tau}_+) - \bar{m}_-(t - \bar{\tau}_-) \}. \quad (1)$$

Time-base distortion

Because of timing errors in the receiving oscilloscope, signals are sampled at unequally spaced intervals. At the p th sample, the timing error is the sum of a deterministic time-base distortion $TBD(p)$ and a random timing jitter error τ_p . Thus, the p th sample of the signal of interest is $\hat{m}(t_0 + (p-1)\Delta + TBD(p) + \tau_p) + \varepsilon_p$, where ε_p is additive noise, Δ is the target time interval between samples, and t_0 may depend on instrument drift. The expected mean value of the jitter and additive noise is zero.

Errors due to TBD necessitate compensation to give good electrical mismatch corrections above about 15 GHz. We developed an efficient least-squares algorithm⁵ for estimating TBD. The method requires measurements of sinusoidal signals at two phases and two frequencies. It can accurately estimate the order of the harmonic model that is used to account for the amplitude nonlinearity of the sampler and separate the effect of the nonlinearity from the TBD estimate. To improve the TBD estimate we average results from 100 sets of waveforms. Each set of four waveform measurements contains a 9.75 GHz signal and nearly quadrature signal, and a 10.25 GHz signal and nearly quadrature signal. The sinusoidal signals are generated using an inexpensive 100 kHz-3.2 GHz synthesized signal generator, whose 5 MHz reference is provided by a Hydrogen maser that is maintained by the NIST Time and Frequency Division. The synthesized signal is multiplied by a $5\times$ multiplier and is amplified and filtered to ensure spurious harmonics of the input signal less than -60 dB (re: carrier) and spurious harmonics of the output signal less than -50 dB (re: carrier). The oscilloscope is triggered using the fundamental signal generated by the signal generator, and the relative phase of the measured waveform is set by changing the trigger level of the oscilloscope. Acquisition of 100 sets of four waveforms takes about 10 minutes and includes time for letting the signal generator settle after switching frequencies.

Our least squares algorithm can be used with weighting to estimate TBD. We begin with a set of equal weights, and then estimate the TBD, amplitude, and phase parameters. With these estimates in hand, we compute the residuals of the fit and then use the inverse of the squared residuals as a new set of weights to obtain the TBD and other parameters. This process is repeated until it converges. Simulation studies show that the bias of the TBD estimate obtained from 100 sets of waveforms is very small, thus the variation

among the 100 individual TBD estimates is a good measurement for the uncertainty of the TBD estimate. Since repeated measurements are available, we have also developed a method that can be used to reduce the bias of the jitter σ_τ and additive noise σ_ϵ estimates. Specifically, under the assumptions of Gaussian jitter errors and negligible harmonic distortion, we have shown that

$$\sigma_y^2 = \frac{A^2}{2} \left(1 + e^{-8\pi^2 f^2 \sigma_\tau^2} - 2e^{-4\pi^2 f^2 \sigma_\tau^2} \right) + \sigma_\epsilon^2 + (g'(t_i))^2 \sigma_\tau^2 \left(\frac{e^{-4\pi^2 f^2 \sigma_\tau^2} - e^{-8\pi^2 f^2 \sigma_\tau^2}}{4\pi^2 f^2 \sigma_\tau^2} \right), \quad (2)$$

where A is the amplitude and f is the frequency of the sinusoidal signal, and $g'(t_i)$ is the derivative of the measured sinusoid after TBD correction. The result can be used to adjust for the bias of additive and jitter variance estimates obtained by the first-order approximation. These biases can be large if σ_τ^2 is not small.

Based on the estimated time-base distortion, we approximate our signal of interest using a regression spline model⁶. We sample this continuous time representation of the unequally spaced observed signal at equally spaced times. Fourier analysis is done on this interpolated signal to implement further corrections.

Adapter mismatch correction

We perform mismatch correction in the frequency-domain because multiple reflections between the receiver and generator can not be windowed out in time. The mismatch correction is found using the flow diagram shown in Fig. 3. If the samplers were ideal, reflectionless, and connected with an ideal adapter, the measured waveform would be $M_{ij}(\omega) \propto H_i(\omega) K_j(\omega)$, where $H_i(\omega)$ is the frequency-domain representation of the impulse response of the receiver and $K_j(\omega)$ is the kick-out waveform. Instead, the waveform $\hat{M}_{ij}^{TBD}(\omega)$, which is already

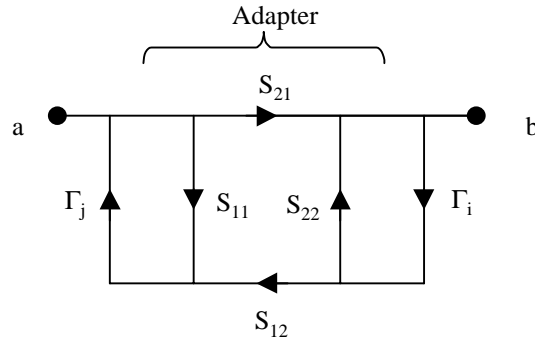


Fig. 3. Flow diagram used to calculate mismatch correction factor $r_{ij}=b/a$.

corrected for TBD and drift, must additionally be corrected for the adapter network by dividing by r_{ij} , given by

$$r_{ij} = \frac{S_{21}}{1 - S_{11}\Gamma_j - S_{22}\Gamma_i - \Gamma_i\Gamma_j(S_{21}S_{12} - S_{11}S_{22})}, \quad (3)$$

where S_{xy} refers to the measured frequency-dependent S-parameters for the adapter used to connect the two samplers (i and j), and Γ_x is the measured frequency-dependent reflection coefficient for the x th sampler. We have found that if the $M_{ij}(\omega)$ are not corrected for TBD prior to mismatch correction, the mismatch correction has little or no effect above about 20 GHz.

Jitter

The effect of jitter on an averaged signal is that of a lowpass filter⁷. The variance of the measured signal can be expressed in a Taylor-series expansion as

$$\sigma_{Total}^2 \approx \sigma_N^2 + \sigma_J^2 \left(\frac{dV}{dt} \right)^2, \quad (4)$$

where σ_{Total}^2 is the total measured signal variance, σ_N^2 is the additive noise variance, σ_J^2 is the jitter variance, and dV/dt is the derivative of the ideal time-domain waveform. We are currently investigating methods for estimating these quantities. Typically $\sigma_J \approx 1.1-1.2$ ps and is assumed to be normally

distributed. The estimated $H_j(\omega)$ is then multiplied by $\exp(\sigma_j^2\omega^2/2)$ over the frequency range of interest to deconvolve the jitter effects.

Measurement results

Since the n2n method is based on the assumption that $K_i(\omega) \propto H_i(\omega)$, the response of each of the three samplers can be estimated using the corrected measurements:

$$H_j^{est}(\omega) = C\sqrt{K_j(\omega)H_j(\omega)}$$

$$= C\exp(\frac{1}{2}\sigma_j^2\omega^2)\sqrt{\frac{\hat{M}_{ij}^{TBD}(\omega)\hat{M}_{jk}^{TBD}(\omega)}{\hat{M}_{ik}^{TBD}(\omega)}\frac{r_{ik}(\omega)}{r_{ij}(\omega)r_{jk}(\omega)}}, \quad (5)$$

where C is an arbitrary constant and we assume that the jitter is the same for all three M_{xy} measurements. The square root in the second part of equation 5 is taken by unwrapping and detrending the phase of the complex product inside the radical and dividing by 2.

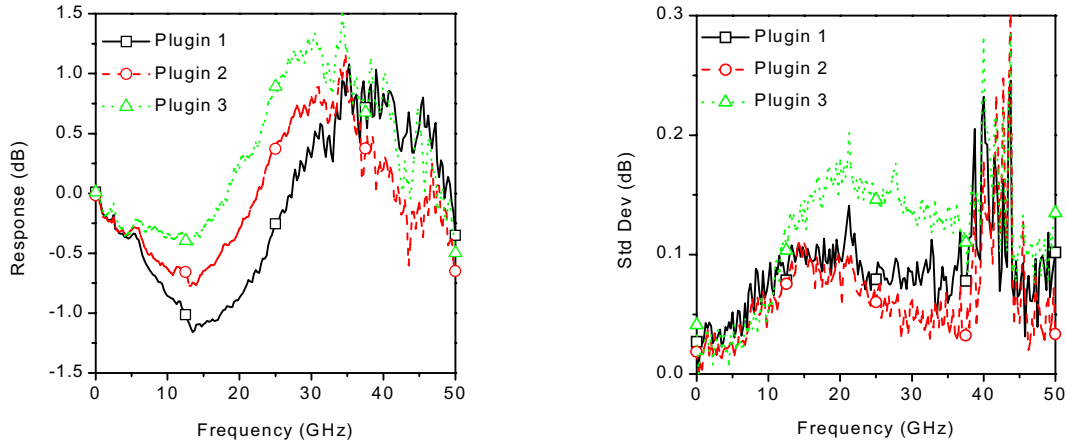


Fig. 4. Mean and standard deviation of the response magnitude ($|H(\omega)|$) for 5 measurements on an ensemble of 3 samplers.

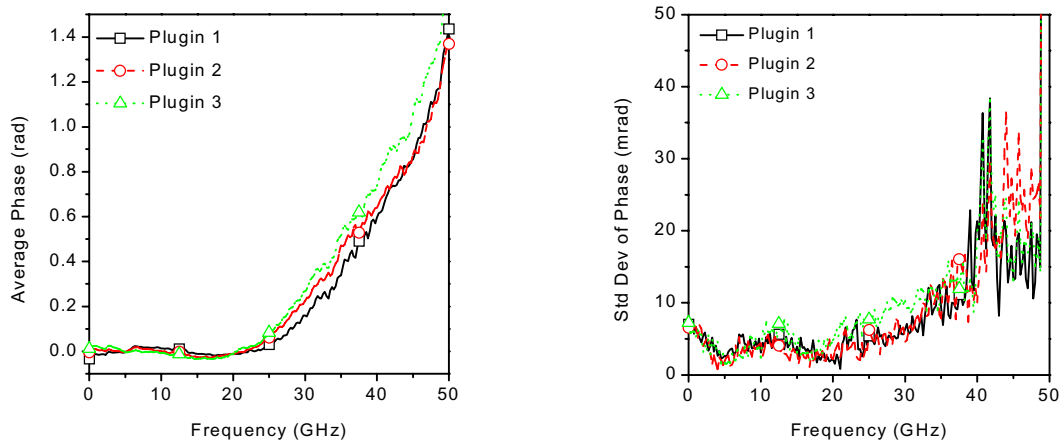


Fig. 5. Mean and standard deviation of the response phase ($\arg(H(\omega))$) for 5 measurements on an ensemble of 3 samplers.

Figures 4 and 5 show the measured mean and standard deviation of the frequency response magnitude and phase for 5 measurements of an ensemble of 3 samplers. For each measurement, the waveform pairs for each sampler combination are measured 1000 times. The waveforms are measured over a 4 ns time epoch with 1.953 ps between each sample. Extending the measured time epoch does not add significant information to the measurement. Finer resolution in the frequency range could be calculated synthetically by padding the transformed estimated response with zeroes and performing the inverse transform. For this study the frequency grid is determined by the time epoch of the measured data. We estimate the linear portion of the phase using a least-squares fit between 0 and 20 GHz. The linear portion of the phase is subtracted before determining the mean and standard deviation.

Differences between the curves show that the response of each sampler is different, yet repeatable. The variability of the magnitude response may be acceptable for many applications up to about 38 GHz. Resonances in the response seem to reduce repeatability in the region from 40 to 45 GHz. In general, the phase variability increases for frequencies above 20 GHz. Although the magnitude variability is somewhat high relative to standard vector network analyzer measurements, the phase variability is fairly small. This is a desirable result since our main goal in n2n calibration is the phase response.

The procedure we have described is intended to estimate the frequency-domain properties of the oscilloscope sampler. Clearly there are several places in this procedure where the correction factors are determined over a specific frequency range with data cut-off above 50 GHz. The effect of the band-limited data is to add ringing in the time-domain that may be undesirable for some applications.

Comparison to swept sine-wave measurements

As a verification of the n2n calibration of magnitude response, we performed swept sine-wave measurements to compare the response of the oscilloscope to that of a calibrated thermoelectric power meter. The setup for this measurement is shown in Fig. 6. Measurements were performed between 1 and 50 GHz. The generator power was set at -3 dB (re: 1 mW) at 1 GHz with an increase of 0.08 dB/GHz. The receiving oscilloscope was placed in vertical histogram mode to measure the standard deviation (and variance) of the voltage. The measured power is calculated as

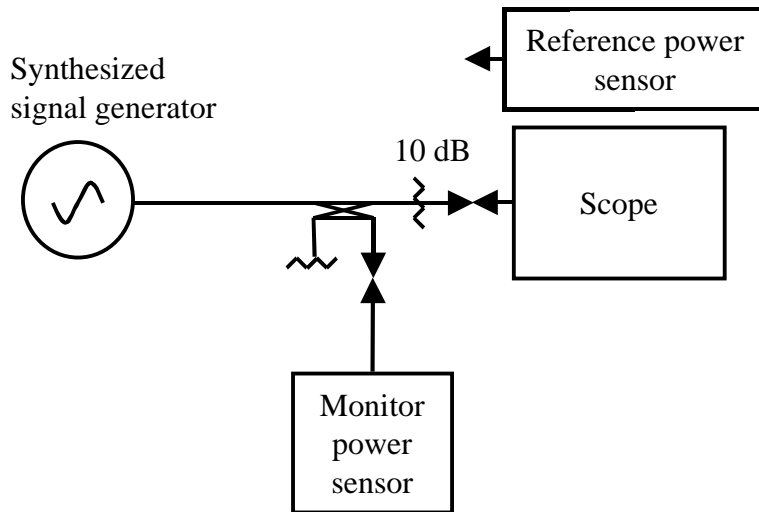


Fig. 6. Schematic of experimental configuration for swept sine-wave measurements of oscilloscope sampler response.

$$P_{scope} = \frac{1}{50 \Omega} (\sigma_S^2 - \sigma_B^2), \quad (6)$$

where σ_S^2 is the signal variance measured during the scan, and σ_B is the background variance measured before the scan. The magnitude response of the scope is then found as⁸

$$20\log(H(\omega)) = 10\log\left(\frac{P_{scope} P_{mon}}{P_{mon}' P_{meter}} k \left\{ \frac{|1 - \Gamma_g \Gamma_{scope}|^2}{|1 - \Gamma_g \Gamma_{meter}|^2} \right\}\right), \quad (7)$$

where

P_{mon}' = monitor power meter reading while measuring scope

P_{mon} = monitor power meter reading while measuring power meter standard

P_{meter} = standard power meter reading

k = calibration factor of standard power meter = $\eta(1 - |\Gamma_{meter}|^2)$

η = standard power meter substitution efficiency

Γ_{meter} = electrical reflection coefficient of the standard power meter

Γ_g = equivalent source electrical reflection coefficient⁹.

The part in curly braces is treated as a mismatch uncertainty, instead of as a full correction. The result of a swept sine-wave measurement on a typical sampler compared with the n2n measurement is shown in Fig. 7. The n2n measurements are consistently larger than the swept-sine measurements. This is consistent with the results reported by Verspecht and Rush¹. Simulations have also shown that n2n measurements may give high estimates of the magnitude response^{3,4}.

Conclusions

In conclusion, we have implemented experimental and computational procedures for nose-to-nose calibration. Our procedures include new methods for drift correction and TBD correction. We remove effects due to the adapter propagation delay and mismatch and correct for jitter. The variation in our phase estimate is quite small, while the variation in magnitude is somewhat larger. We compared the magnitude response measured by nose-to-nose calibration with a power meter measurement and found a significant discrepancy, comparable to that reported by the inventors, Verspecht and Rush¹. We still lack a method for verifying the total phase, although we have not found any evidence that indicates the nose-to-nose method is failing.

Acknowledgments

We gratefully acknowledge Frans Verbeyst, Marc Vanden Bossche, and Jan Verspecht who developed the nose-to-nose theory and practical implementation, and have patiently guided us through their work, both published and unpublished. We also thank Kate Remley for providing Fig. 1 and for useful insight into operation of the sampler. Part of this work was supported by the Office of Naval Research and the Space and Naval Warfare Systems Center.

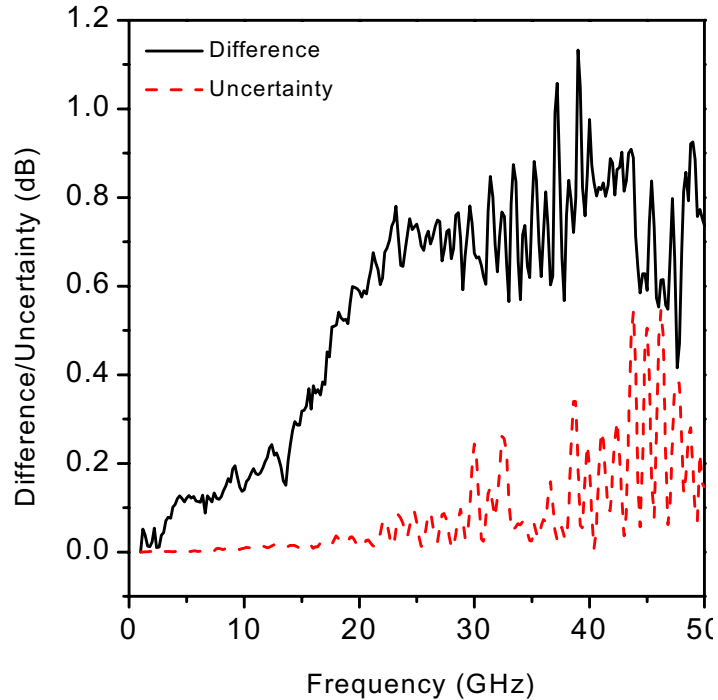


Fig. 7. Difference between nose-to-nose measurement and swept sine-wave measurement. Uncertainty is calculated by summing the part of eq. 7 in curly braces with the repeatability of the nose-to-nose measurement in quadrature. Uncertainties for other systematic errors are not included.

References

- ¹ J. Verspecht and K. Rush, "Individual characterization of broadband sampling oscilloscopes with a 'nose-to-nose' calibration procedure," *IEEE Trans. Instrum. Meas.*, vol. 43, pp. 347-354, 1994.
- ² J. Verspecht, "Broadband sampling oscilloscope characterization with the nose-to-nose calibration procedure: a theoretical and practical analysis," *IEEE Trans. Instrum. Meas.*, vol. 44, pp. 991-997, 1995.
- ³ D. F. Williams, K. A. Remley, and D. C. DeGroot, "Nose-to-nose response of a 20 GHz sampling circuit," *54th ARFTG Conference Digest*, Dec. 1999, pp. 64-70.
- ⁴ K. A. Remley, D. F. Williams, and D. C. DeGroot, "Realistic sampling circuit model for nose-to-nose simulation," *IMS Conference Digest*, June, 2000.
- ⁵ C. M. Wang, P. D. Hale, and K. J. Coakley, "Least-squares estimation of time-base distortion of sampling oscilloscopes," *IEEE Trans. Instrum. Meas.*, vol. 48, pp.1324-1332, 1999.
- ⁶ Y. Rolan, J. Schoukens, and G. Vandersteen, "Signal reconstruction for nonequidistant finite length sample sets: a KIS approach," *IEEE Trans. Instrum. Meas.*, vol. 47, pp. 1046-1052, 1998.
- ⁷ W. L. Gans, "The measurement and deconvolution of time jitter in equivalent-time waveform samplers," *IEEE Instrum. Meas.*, vol. 32, pp 126-133, 1983.
- ⁸ D. C. DeGroot, P. D. Hale, M. Vanden Bosche, F. Verbeyst, and J. Verspecht, "Analysis of interconnection networks and mismatch in the nose-to-nose calibration," *55th ARFTG Conference Digest*, June 2000.
- ⁹ J. R. Juroshek, "A direct calibration method for measuring equivalent source mismatch," *Microwave J.*, Oct. 1997, pp. 106-118.